

Electron Transfer Properties of Bisphenol Derivatives in Relation to Their Developing Properties in Silver Salt Photothermographic Systems

Hiromi Akahori, Kiyokazu Morita, Ayumu Nishijima, and Tsuyoshi Mitsunashi

R&D Center, Medical & Graphic Company, Konica Corporation, Hino, Tokyo, Japan

Kei Ohkubo and Shunichi Fukuzumi

Department of Material and Life Science, Graduate School of Engineering, Osaka University, CREST, Japan Science and Technology Corporation (JST), Suita, Osaka, Japan

Electron transfer properties of a series of bisphenol derivatives were examined in relation to their developing properties in silver salt photothermography. A *t*-butyl-substituted bisphenol derivative exhibited the highest developing reactivity among bisphenol derivatives investigated in this study. The substituent effects of bisphenol derivatives on the one-electron oxidation potentials and the rates of electron transfer with one-electron oxidants have revealed that the deprotonation step from the bisphenol radical cation, to produce a phenoxyl radical, plays an important role in determining the overall oxidation reactivity in the two-electron oxidation process. The ESR spectra of phenoxyl radicals derived from bisphenol derivatives indicate formation of an intramolecular hydrogen bond between oxygen and OH group of phenoxyl radicals. The reactivity of the bisphenol derivatives during the oxidation process is controlled by the hydrogen bond formation. The high oxidation reactivity of the *t*-butyl-substituted bisphenol derivative is ascribed to its low ionization potential and low deprotonation energy, as compared with the other alkyl-substituted bisphenol derivatives.

Journal of Imaging Science and Technology 47: 124–132 (2003)

Introduction

Photothermographic materials utilizing silver halides and silver carboxylates have been widely used in dry processing imaging systems where latent images are produced on the surfaces of silver halide particles. The latent image is transformed into developed metallic silver by the reduction of silver ions provided by silver carboxylates.^{1,2} The silver ion transport and reduction process has been proposed to consist of three steps.² In the first step, silver carboxylates may react with phthalic acid to produce silver phthalate, which then reacts with phthalazine to produce a silver phthalazine complex. In a subsequent step, metallic silver is produced in the presence of the latent image by the reduction of silver ions with a developer. In order to optimize the photothermographic properties of the system, it is essential to control the reactivity of the developer reagent. Bisphenol derivatives have been found to be efficient developers in a photothermographic system, while the important role of bisphenol derivatives as antioxidants and stabilizers have been reported.^{12,13} However, very little is known about the effect of the chemical structure of developing reagents on the developing properties in terms of the electron transfer properties and the oxidation mechanism.

We report herein the fundamental redox properties of bisphenol derivatives such as the one-electron oxidation potentials (E^0_{ox}) and the kinetic analysis of electron transfer oxidation of bisphenol derivatives to reveal the oxidation mechanism in relation to their developing properties in silver salt photothermography. We adopted 1-bis(2-hydroxy-3,5-dimethylphenyl)-3,5,5-trimethylhexane as a reference compound, which has frequently been used as a developer, to examine the electron transfer properties of four bisphenol derivatives with different substituents (methyl, ethyl, *n*-propyl, and *t*-butyl groups) neighboring the hydroxyl groups. A proposed mechanism for the two-electron oxidation of this compound is shown in Scheme 1. ESR spectra of phenoxyl radicals which are oxidation intermediates derived from bisphenol derivatives are also reported, providing valuable insight into the role of intramolecular hydrogen bond in the oxidation processes.

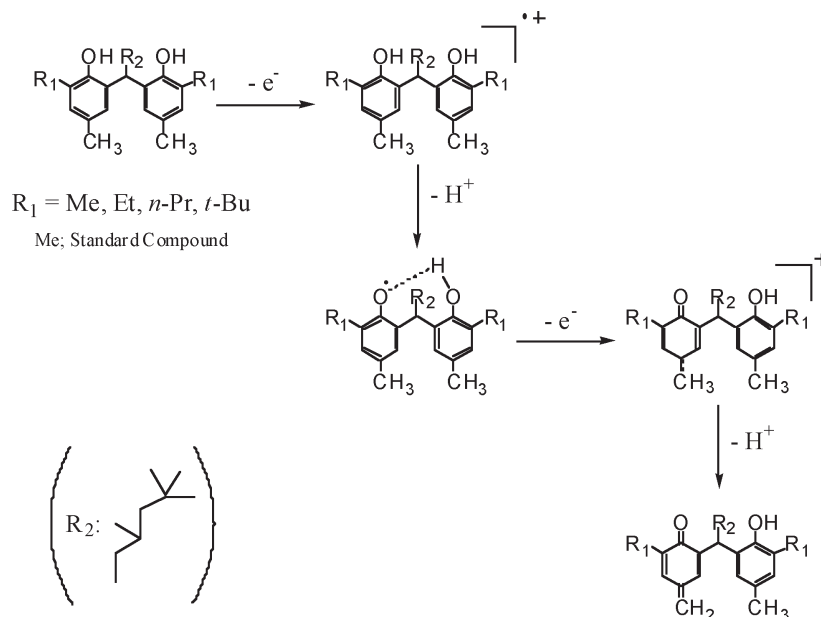
Experimental Section

Materials

1-Bis(2-hydroxy-3,5-dimethylphenyl)-3,5,5-trimethylhexane was obtained commercially and purified by the standard method.³ The other bisphenol derivatives were prepared according to the literature⁴ and purified by the standard methods.³ A one-electron oxidant used in this study, tris(2,2'-bipyridine)iron(III) hexafluorophosphate [$\text{Fe}(\text{bpy})_3](\text{PF}_6)_3$], was prepared according to the literature.⁵ Tetrabutylammonium perchlorate (TBAP), obtained from Fluka Fine Chemical, was recrystallized from ethanol and dried in vacuo prior to use. Acetonitrile (MeCN; spectral grade) was purchased

Original manuscript received September 27, 2002

©2003, IS&T—The Society for Imaging Science and Technology



Scheme 1.

from Nacalai Tesque and used as received. Di-*t*-butyl peroxide was purchased from Nacalai Tesque and purified by the standard method.³ Dichloromethane (CH₂Cl₂; spectral grade) was purchased from Wako Pure Chemical Industries and used as received.

Electrochemical Measurements

Electrochemical measurements were performed on a BAS 100B electrochemical analyzer (Bioanalytical Systems, Inc./USA) in acetonitrile (MeCN) containing 0.10 M TBAP as a supporting electrolyte at 298K. A conventional three-electrode cell was with a gold working electrode and a platinum wire as the counter electrode. The gold working electrode was polished with a BAS polishing alumina suspension and rinsed with acetone before use. The measured potentials were recorded with respect to the Ag/AgNO₃ (0.01M) reference electrode. All potentials (versus Ag/Ag⁺) were converted to values versus SCE by adding 0.29 V.⁶ The one-electron oxidation potential (E_{ox}^0) of ferrocene used as a standard is 0.37 V versus SCE in MeCN under our experimental conditions.

Kinetic Measurements

Kinetic measurements of the oxidation of the bisphenol derivatives with [Fe(bpy)₃](PF₆)₃ in MeCN were performed on a UNISOKU RSP-601 stopped-flow rapid scan spectrophotometer (UNISOKU/Japan) with a MOS-type high sensitivity photodiode array, at 298K. All kinetic measurements were carried out under conditions where the concentration of [Fe(bpy)₃](PF₆)₃ was maintained at >10-fold excess relative to that of the bisphenol derivatives. Rates of the oxidation of bisphenol derivatives with [Fe(bpy)₃](PF₆)₃ in MeCN were monitored by measuring the increase in absorbance due to [Fe(bpy)₃]²⁺ at $\lambda_{\text{max}} = 520 \text{ nm}$ ($\epsilon_{\text{max}} = 8.7 \times 10^3 \text{ M}^{-1} \text{ cm}^{-1}$) in MeCN at 298K.⁷ The pseudo-first-order rate constants were determined by least-squares curve fitting using a personal computer.

ESR Measurements

ESR measurements were performed on a JEOL X-band spectrometer (JES-ME-LX) under photoirradiation of a deaerated CH₂Cl₂ solution containing di-*t*-butyl peroxide (ca. 0.5 M) and a bisphenol derivative (ca. 0.2 M) with a 1000 W mercury lamp at 298K. The magnitude of the modulation was chosen to optimize the resolution and the signal to noise ratio (S/N) of the observed spectra under nonsaturating microwave power conditions. The *g* values were calibrated using a Mn²⁺ marker and the hyperfine coupling constants were determined by computer simulation using a Calleo ESR (version 1.2) program coded by Calleo Scientific Software Publishers (Colorado, USA) on a Macintosh personal computer.

Theoretical Calculations

The density functional theory (DFT) calculations were performed at the Becke3LYP/6-31G or BeckeLYP/3-21G level^{8,9} with Gaussian 98 program on a COMPAQ DS20E computer.

Evaluation of Photographic Properties (Sensitometry)

The evaluation of photographic properties was performed following a standard procedure: the film samples comprising organic silver salts, silver halide grains and other reagents were prepared according to the literature.¹⁰ They were uniformly exposed with a 810 nm laser diode, and developed at a typical thermal development temperature of 399K. Both exposure and development were performed on Konica DRYPRO™ MODEL 722.

Analyses of Oxidation Products in Film

LC/MS was used to analyze the oxidation products of the bisphenol derivatives in the films. After thermal development, these reaction products in the film were extracted with methanol in HCl (4 N) mixed solvent and analyzed using the on-line LC/MS method.

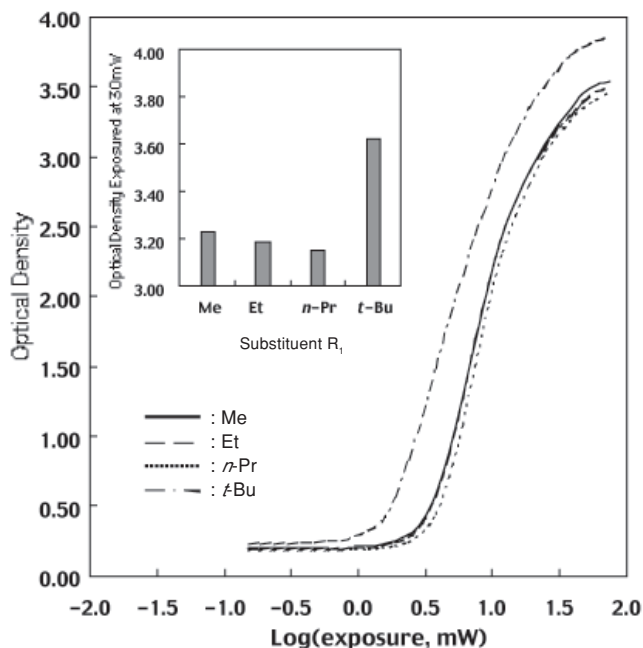


Figure 1. Effects of substituents of bisphenol derivatives on photothermographic characteristic curves obtained by development at 399K.

Results and Discussion

Photographic Properties (Sensitometry)

Figure 1 shows the characteristic curves of the film samples to which various bisphenol derivatives were added. The developing rate of substituted bisphenols slightly decreased with the substituent in order: *t*-butyl, methyl, ethyl, and *n*-propyl.

During the course of development, the bisphenol derivative is oxidized to various oxidation states. The oxidation products were analyzed using LC/MS. As shown in Scheme 2, not only a two-electron oxidized product, but also four-, six-, eight-, ten-, and twelve-electron oxi-

TABLE I. One-Electron Oxidation Potentials (E^0_{ox}) of Bisphenol Derivatives in MeCN

R_1	E^0_{ox} (versus SCE, V)
Me	1.14
Et	1.15
<i>n</i> -Pr	1.15
<i>t</i> -Bu	1.18

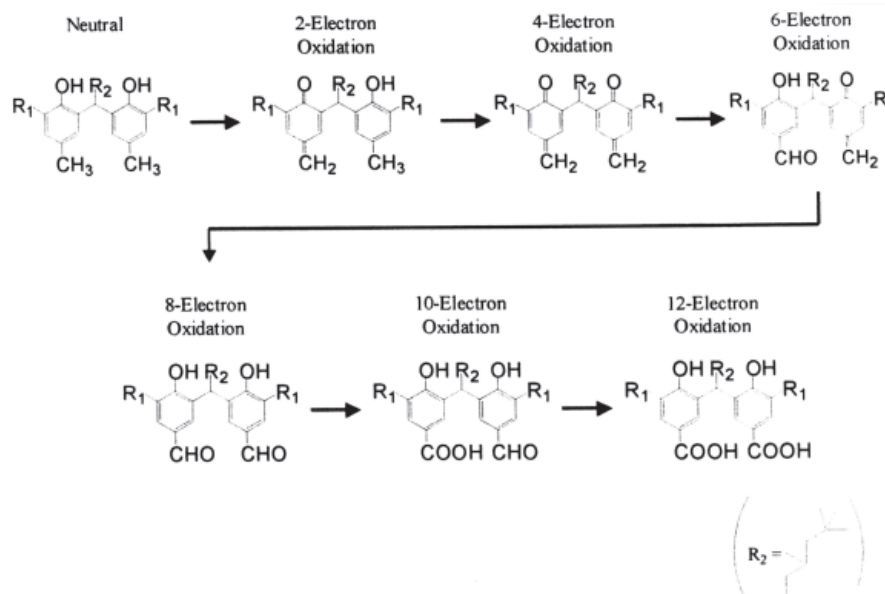
dized products were detected starting from a bisphenol derivative. The relative yields of oxidation products at a given exposure were determined as the HPLC peak area. A decrease in the starting material, an increase in the two-electron, four-, six-, eight-, ten-, and twelve-electron oxidation products during the course of development are shown in Fig. 2 (a-g, respectively). In the case of the *t*-butyl derivative, the two-electron oxidation products are dominant and a decrease in the starting material is the fastest, as compared with the other bisphenol derivatives.

Electron Transfer Properties

The differential pulse voltammograms of bisphenol derivatives were measured in MeCN. The one-electron oxidation potentials (E^0_{ox} versus SCE) of four different bisphenol derivatives thus determined are listed in Table I, where the E^0_{ox} value is relatively constant and invariant regardless of the difference in substituents of bisphenol derivatives.

The electron transfer oxidation of bisphenol derivatives was examined using the one-electron oxidant, $[\text{Fe}(\text{bpy})_3](\text{PF}_6)_3$. Upon mixing a bisphenol derivative and $[\text{Fe}(\text{bpy})_3](\text{PF}_6)_3$ in MeCN, $[\text{Fe}(\text{bpy})_3]^{3+}$ is reduced by a bisphenol derivative as indicated by appearance of the absorption band at 520 nm due to $[\text{Fe}(\text{bpy})_3]^{2+}$ (Fig. 3). The spectral titration indicates that each bisphenol derivative is oxidized by two equivalents of $[\text{Fe}(\text{bpy})_3]^{3+}$ to give a two-electron oxidation product at the initial reaction stage (Scheme 3).

Since the electron transfer rate was too fast to follow using a conventional spectrophotometer, a stopped-flow technique was employed to determine the rate.



Scheme 2.

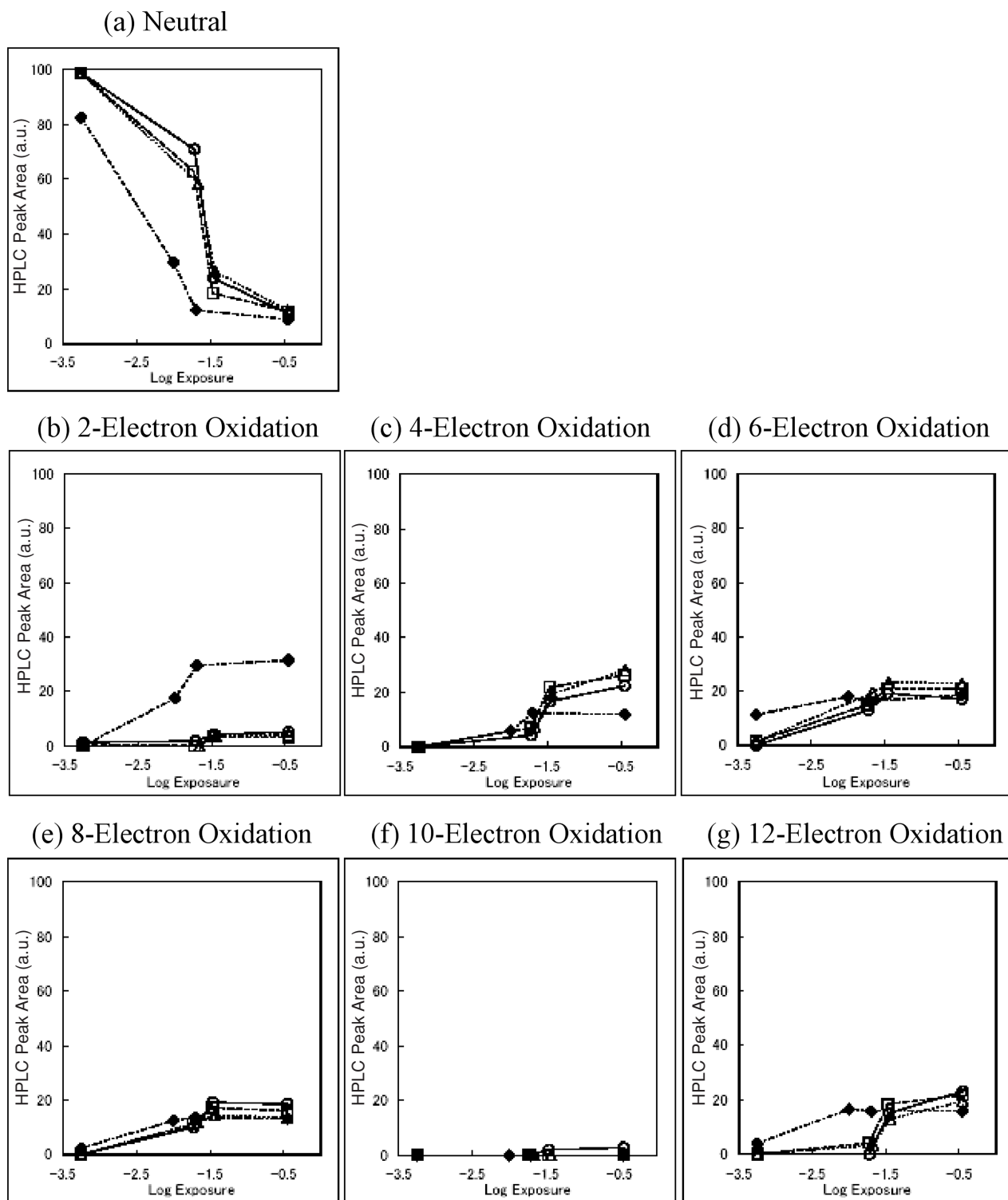
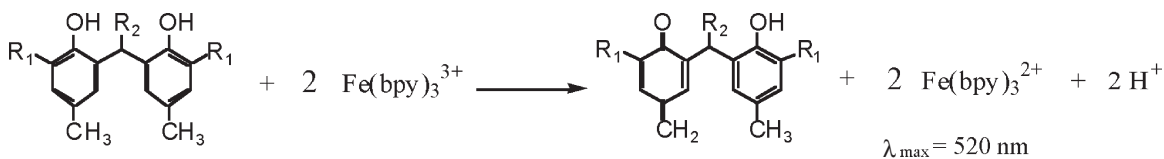


Figure 2. The relative yields of oxidation products at a given exposure in the film containing bisphenol derivatives; $R_1 = \text{Me}$ (○), $R_1 = \text{Et}$ (Δ), $R_1 = n\text{-Pr}$ (□), and $R_1 = t\text{-Bu}$ (◆).



Scheme 3.

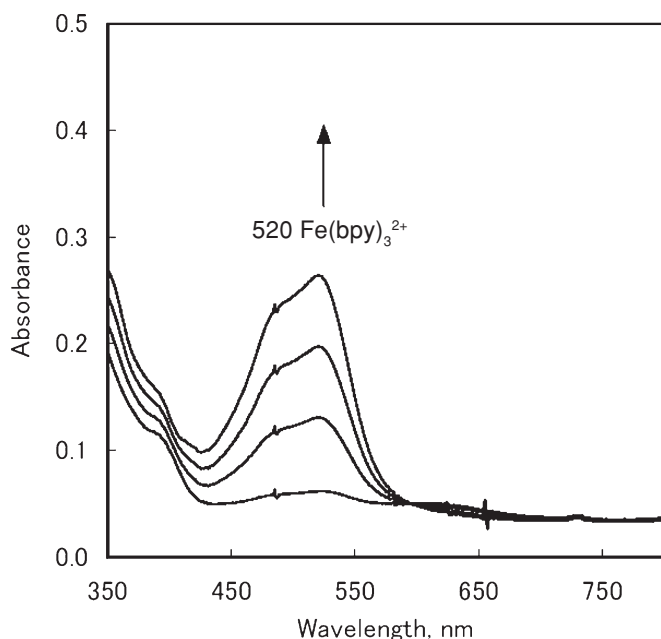


Figure 3. Visible spectral change observed in the titration of $[\text{Fe}(\text{bpy})_3](\text{PF}_6)_3$ (4.95×10^{-5} M) with a bisphenol derivative ($R_1 = \text{Me}$) in MeCN at 298 K; concentration of bisphenol derivative: 0, 3.19, 6.19 and 9.01 μM .

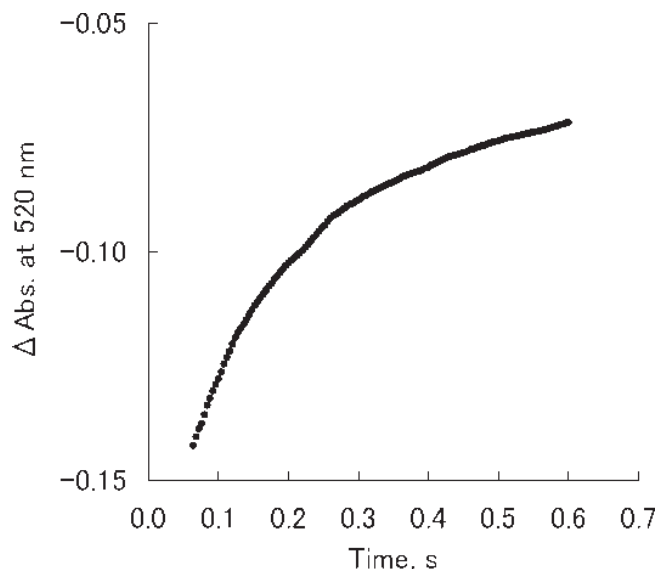


Figure 4. Time dependence of absorbance at 520 nm due to $[\text{Fe}(\text{bpy})_3]^{2+}$ in electron transfer from a bisphenol derivative ($R_1 = \text{Me}$, 3 μM) to $[\text{Fe}(\text{bpy})_3](\text{PF}_6)_3$ (3×10^{-4} M) recorded on a stopped-flow spectrophotometer with 10 mm cell in MeCN at 298 K; the ϵ_{max} of $[\text{Fe}(\text{bpy})_3]^{2+}$ is $8.7 \times 10^3 \text{ M}^{-1} \text{ cm}^{-1}$.

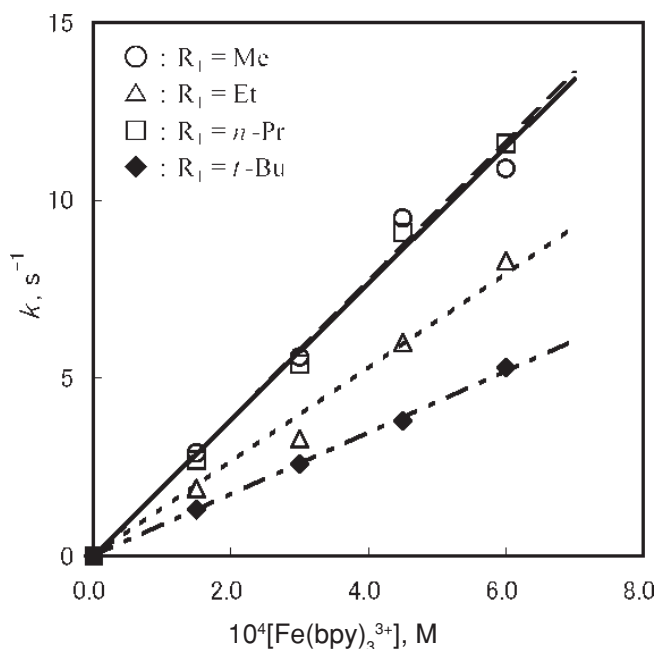


Figure 5. Plots of pseudo-first order rate constant (k) versus $[\text{Fe}(\text{bpy})_3]^{3+}$ in the two-electron transfer oxidation of bisphenol derivatives (3 μM) with $[\text{Fe}(\text{bpy})_3]^{3+}$ in MeCN at 298 K.

Figure 4 shows the dynamics of the two-electron oxidation of a bisphenol derivative in MeCN monitored by the rise in absorbance due to $[\text{Fe}(\text{bpy})_3]^{2+}$. The rate obeys pseudo-first order kinetics and the pseudo-first order rate constant (k) exhibits first order dependence with respect to the $[\text{Fe}(\text{bpy})_3]^{3+}$ concentration used in excess, as shown in Fig. 5. The slope gives the second

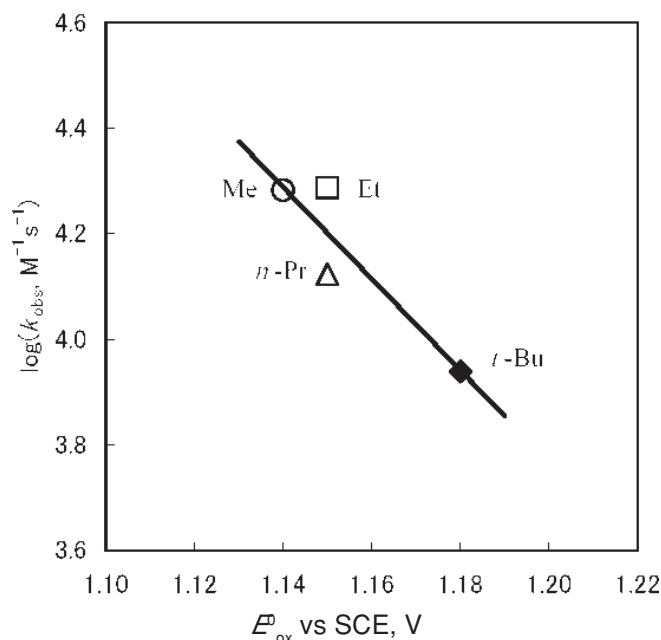
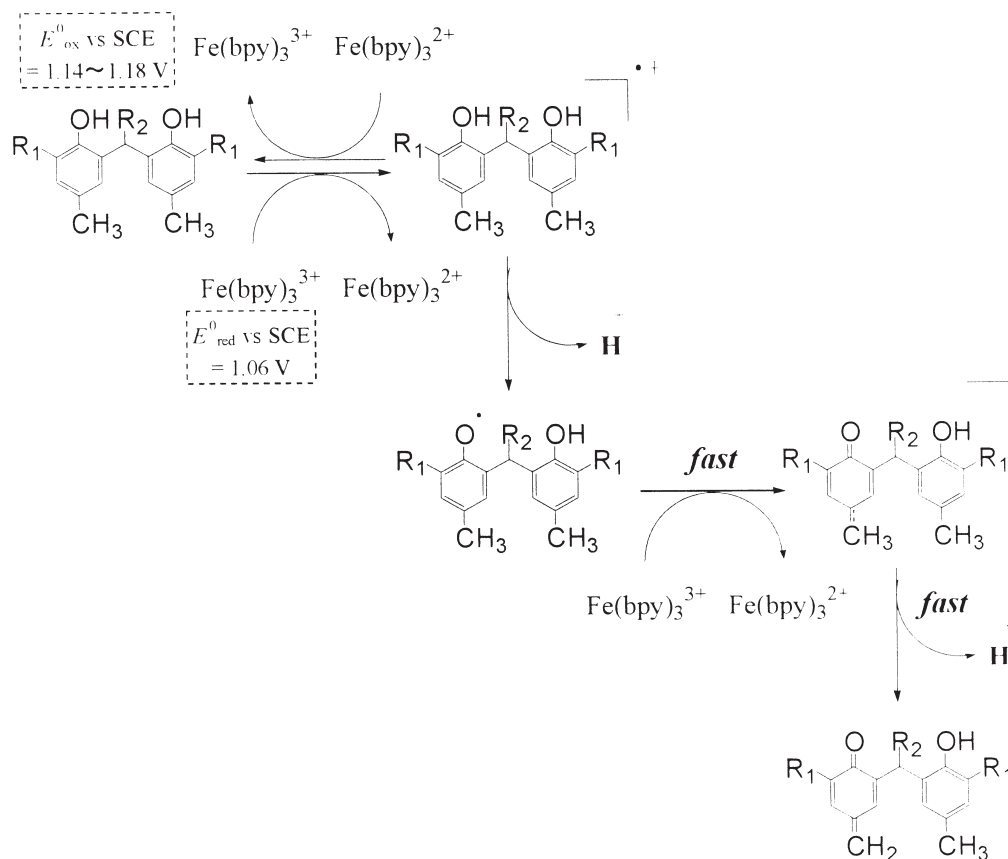


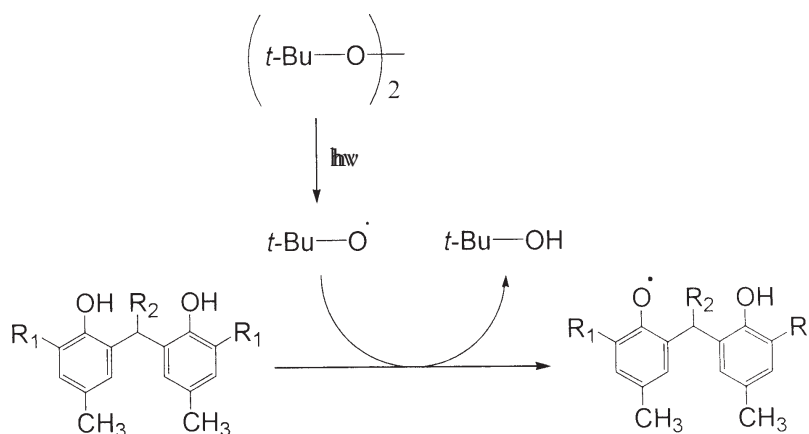
Figure 6. Plots of $\log k_{\text{obs}}$ versus E^0_{ox} ; the correlation between logarithm of the observed second order rate constants for the two-electron oxidation of bisphenol derivative and the one-electron oxidation potentials in MeCN.

order rate constant (k_{obs}) for the two-electron oxidation process in MeCN.

Figure 6 shows that the correlation between the logarithm of the observed second-electron rate constants ($\log k_{\text{obs}}$) of the two-electron oxidation of the bisphenol derivatives and the one-electron oxidation potentials (E^0_{ox}) in MeCN. Although the difference in k_{obs} and E^0_{ox} of



Scheme 4



Scheme 5

bisphenol derivatives is rather small, there is a clear trend of decreasing k_{obs} with increasing E_{ox}^0 . We infer that the two electron oxidation occurs via the initial electron transfer from a bisphenol derivative to $[\text{Fe}(\text{bpy})_3]^{3+}$ followed by deprotonation of the radical cation of bisphenol derivative and subsequent fast electron transfer from the resulting phenoxyl radical to $[\text{Fe}(\text{bpy})_3]^{3+}$ (Scheme 4). Since the initial electron transfer is endothermic, judging from the oxidation potentials of the bisphenol derivatives and the reduction potential of $[\text{Fe}(\text{bpy})_3]^{3+}$, the deprotonation step may be concerted with the initial electron transfer step. In such a case, the deprotonation step to produce the phenoxyl radical

plays an important role in determining the overall reactivity of the two-electron oxidation process.

Oxidation Intermediates

Oxidation intermediates of bisphenol derivatives, i.e., phenoxyl radical species, as shown in Scheme 4, were produced by hydrogen abstraction from bisphenol derivatives with t -butoxyl radical (*vide infra*). Photoirradiation of a CH_2Cl_2 solution containing di- t -butyl peroxide and a bisphenol derivative with a 1000 W mercury lamp at 298 K affords the corresponding phenoxyl radical. Under photoirradiation, the O-O bond of di- t -butyl peroxide is cleaved to produce a t -butoxyl

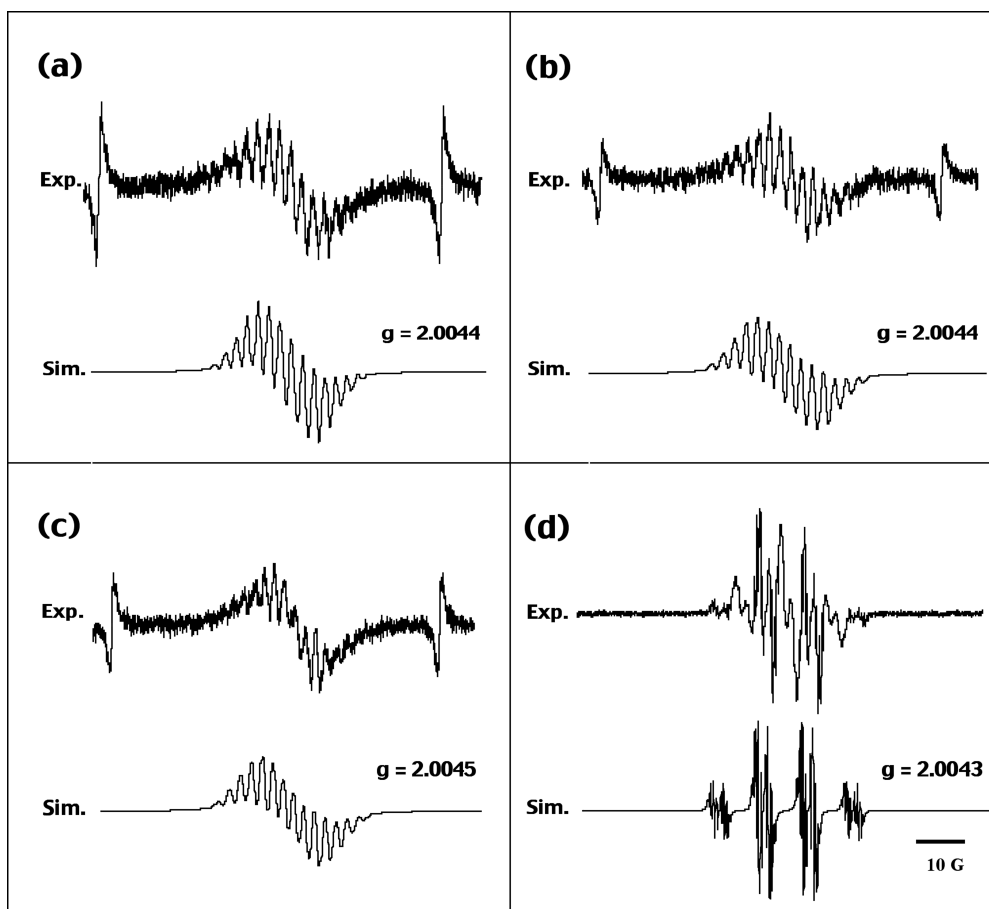


Figure 7. ESR spectra of phenoxyl radicals observed under photoirradiation of deaerated CH_2Cl_2 solutions containing bisphenol derivatives (a) $R_1 = \text{Me}$, (b) $R_1 = \text{Et}$, (c) $R_1 = n\text{-Pr}$, and (d) $R_1 = t\text{-Bu}$ and di-*t*-butyl peroxide at 298 K.

radical which can abstract hydrogen from a bisphenol derivative to produce the phenoxyl radical (Scheme 5).

The ESR spectra of phenoxyl radicals thus produced under photoirradiation are shown in Fig. 7. The g values of the ESR spectra, which are slightly larger than the free spin value due to the spin-orbit coupling at the oxygen atom, are typical for phenoxyl radicals.¹¹ In each case, the hyperfine structure is well resolved. The hyperfine coupling constants (hfc) were determined by comparison of the ESR spectra with the computer simulation spectra. The hfc values thus determined are summarized in Fig. 8. In each case, there is a hyperfine coupling due to the proton of OH group. This indicates that the phenoxyl radical forms a hydrogen bond with the proton of OH group of each bisphenol derivative. The assignment of the hyperfine coupling was made based on comparison with spin densities calculated by means of the density functional method. The results of DFT calculations are summarized in Table II, where the O-H distances in bisphenol derivatives, the radical cations, and the phenoxyl radicals are listed for comparison. The O-H distance of each radical cation is significantly shorter than the corresponding distance in the starting bisphenol derivative. In the phenoxyl radical, the O-H distance becomes even shorter. This indicates that a hydrogen bond is formed upon oxidation of bisphenol derivatives and that the hydrogen bond formation is an

important factor in controlling the oxidation reactivity of the bisphenol derivatives.

The energies of the neutral, radical cation, and phenoxyl radical and the relative ionization energies and deprotonation energies were also calculated as shown in Table III. Both the ionization and deprotonation energies of the *t*-butyl derivative are the smallest among the bisphenol derivatives. This is in sharp contrast with the case of the E^0_{ox} value of the *t*-butyl derivative in MeCN, which is the largest among the bisphenol derivatives. Such a difference is ascribed to the solvation in MeCN, which is the smallest for the *t*-butyl derivative due to the steric effect of the bulky substituent.

Figure 9 shows developing reactivities plotted against calculated relative ionization energies as well as against deprotonation energies. In each case, developing reactivity increases with decreasing ionization energy and deprotonation energy. Thus, we conclude that the developing reactivity is controlled by the ionization energy and the deprotonation energy in the gas phase, rather than the one-electron oxidation potential or the electron transfer reactivity in a polar solvent such as MeCN.

Conclusion

New information regarding the oxidation products of the most common bisphenolic developers used in

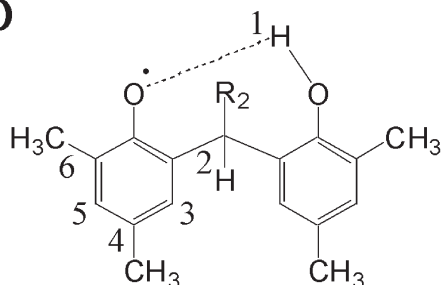
TABLE II. Bonding Distances of the Intramolecular Hydrogen Bond in Various Oxidation States of Bisphenol Derivatives Calculated by the Density Functional Method Using the Gaussian 98 Program (BLYP/3-21G)

R ₁	bonding distance, Å		
	neutral	radical cation	phenoxy radical
Me	1.689	1.496	1.418
Et	1.680	1.482	1.412
<i>n</i> -Pr	1.674	1.481	1.387
<i>t</i> -Bu	1.638	1.463	1.392

TABLE III. Relative Ionization Energies and Relative Deprotonation Energies of Bisphenol Derivatives Calculated by the Density Functional Method Using the Gaussian 98 Program (ROHF/BLYP/3-21G//UHF/BLYP/3-21G)

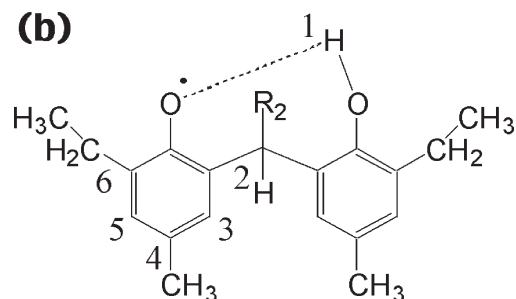
R ₁	relative energy, eV	
	ionization	deprotonation
Me	0.000	0.000
Et	-0.023	-0.004
<i>n</i> -Pr	-0.035	0.001
<i>t</i> -Bu	-0.175	-0.054

(a)



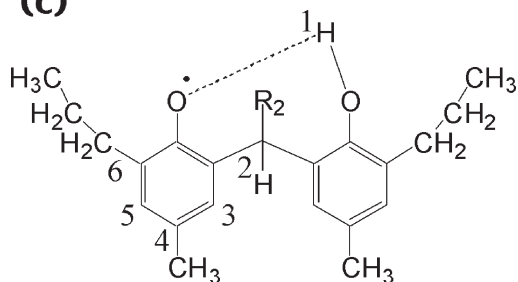
1H (1)	6.00 G	(2.6 G)
1H (2)	2.90 G	(1.3 G)
2H (3, 5)	2.90 G	(2.4, 2.1 G)
3H (4)	5.10 G	(5.7 G)
3H (6)	2.90 G	(3.5 G)

(b)



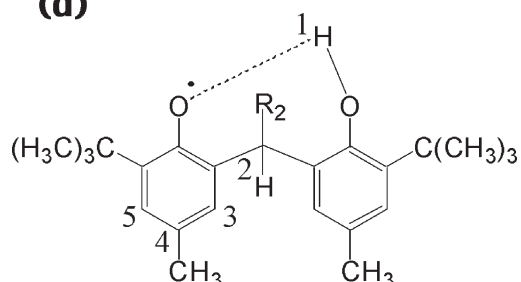
1H (1)	7.70 G	(2.7 G)
1H (2)	3.10 G	(1.2 G)
2H (3, 5)	3.10 G	(2.2, 2.0 G)
3H (4)	5.60 G	(5.6 G)
2H (6)	3.10 G	(1.9 G)

(c)



1H (1)	7.60 G	(2.7 G)
1H (2)	2.80 G	(1.1 G)
2H (3, 5)	2.80 G	(2.3, 2.0 G)
3H (4)	5.60 G	(5.6 G)
2H (6)	2.80 G	(2.1 G)

(d)



1H (1)	3.40 G	(2.7 G)
1H (2)	0.51 G	(1.2 G)
2H (3, 5)	0.75 G	(2.3, 1.9 G)
3H (4)	10.90 G	(5.7 G)

R₂ = 3,3,5-trimethylhexan-1-yl

Figure 8. The hyperfine coupling constants of phenoxy radicals observed under photoirradiation of deaerated CH₂Cl₂ solutions containing bisphenol derivatives (a) R₁ = Me, (b) R₁ = Et, (c) R₁ = *n*-Pr, and (d) R₁ = *t*-Bu and di-*t*-butyl peroxide at 298 K determined by computer simulation using a Calleo ESR version 1.2 program. The values in parentheses are those determined by the DFT calculation using the Gaussian 98 program (BLYP/3-21G).

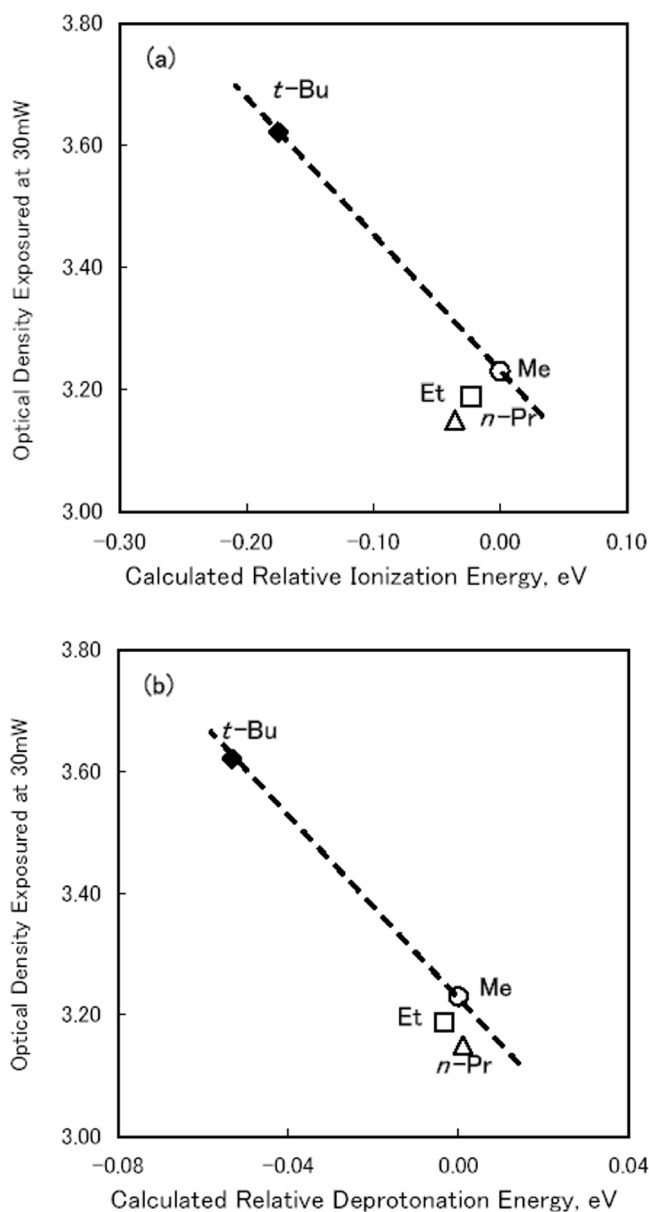


Figure 9. Plots of developing reactivities versus (a) relative ionization energies and (b) relative deprotonation energies calculated by the density functional method using the Gaussian 98 Program (ROHF/BLYP/3-21G//UHF/BLYP/3-21G).

photothremographic products is provided. The conclusions in this work are summarized as follows:

1. An intramolecular hydrogen bond is formed between oxygen and OH group of phenoxy radicals.
2. The reactivity of the bisphenol derivatives during the oxidation process is controlled by the intramolecular hydrogen bond formation.
3. The high oxidation reactivity of *t*-butyl-substituted bisphenol derivative is ascribed to its low ionization potential and low deprotonation energy, as compared with the other alkyl-substituted bisphenol derivatives. \blacktriangle

Acknowledgment. We thank Mr. Y. Endo and Mr. H. Miyao and Mr. N. Miura, Mr. K. Nakamura, and Mr. K. Fukusaka for preparation of reagents in this study, and we thank Mr. H. Yasukawa and Mr. M. Hayakawa for their help in LC/MS measurement and data processing. One of the authors (HA) thanks Mr. G. Reseter and Mr. H. Takiguchi for helpful discussions and comment.

References

1. D. H. Klosterboer, in *Imaging Processes and Materials*, Neblette's Eighth Edition, Ed. J. M. Sturge et al., Van Nostrand-Reinhold, New York, 1989, Chap. 9.
2. Toshihiko Maekawa, Mitsuo Yoshikane, Hidetoshi Fujimura, and Ichizo Toya, *J. Imaging Sci. Technol.* **45**, 365 (2001).
3. D. D. Perrin and W. L. F. Armarego, *Purification of Laboratory Chemicals*, Butterworth-Heinemann, Oxford, 1988.
4. (a) H. E. Ungnade and A. D. McLaren, *J. Amer. Chem. Soc.* **66**, 118 (1944); (b) D. Harper and A. Lambert, GB Patent No. 1,076,142 (1967).
5. (a) C. L. Wong and J. K. Kochi, *J. Amer. Chem. Soc.* **101**, 5593 (1979); (b) S. Fukuzumi, C. L. Wong and J. K. Kochi, *J. Amer. Chem. Soc.* **102**, 2928 (1980).
6. C. K. Mann and K. K. Baenes, *Electrochemical Reactions in Non-aqueous Systems*, Marcel Dekker, New York, 1990.
7. M. H. Ford-Smith and N. J. Sutin, *J. Amer. Chem. Soc.* **83**, 1830 (1961).
8. (a) A. D. Becke, *J. Chem. Phys.* **98**, 5648 (1993); (b) C. Lee, W. Yang and R. G. Parr, *Phys. Rev. B* **37**, 785 (1988).
9. W. J. Hehre, L. Radom, P. v. R. Schleyer, and J. A. Pople, *Ab Initio Molecular Orbital Theory*, Wiley, New York, 1990.
10. Kiyokazu Morita, US Patent No. 6,387,608 (2002).
11. S. Itoh, H. Kumei, S. Nagatomo, T. Kitagawa, and S. Fukuzumi, *J. Amer. Chem. Soc.* **123**, 2165 (2001).
12. L. Taimr, H. Pivcova, and J. Pospisil, *Collect. Czech. Chem. Commun.* **37**, 1912 (1972).
13. L. Taimr and J. Pospisil, *Angew. Macromol. Chem.* **28**, 13 (1973).